

Modeling of Surface Damage at the Si/SiO₂-interface of Irradiated MOS-capacitors

N. Akchurin^a, G. Altopp^b, B. Burkle^b, W. D. Frey^c, U. Heintz^b, N. Hinton^b, M. Hoeferkamp^f, Y. Kazhykarim^a, V. Kuryatkov^d, T. Mengke^a, T. Peltola^{a,*}, S. Seidel^f, E. Spencer^b, M. Tripathi^e, J. Voelker^b

^a*Department of Physics and Astronomy, Texas Tech University, 1200 Memorial Circle, Lubbock, U.S.A*

^b*Department of Physics, Brown University, 182 Hope Street, Providence, U.S.A.*

^c*McClellan Nuclear Reactor Center, University of California Davis, 5335 Price Ave, Davis, U.S.A.*

^d*Nanotech Center, Texas Tech University, 902 Boston Ave, Lubbock, U.S.A.*

^e*Physics Department, University of California Davis, 1 Shields Ave, Davis, U.S.A.*

^f*Department of Physics and Astronomy, University of New Mexico, 1919 Lomas Blvd, Albuquerque, U.S.A*

Abstract

Surface damage caused by ionizing radiation in SiO₂ passivated silicon particle detectors consists mainly of the accumulation of a positively charged layer along with trapped-oxide-charge and interface traps inside the oxide and close to the Si/SiO₂-interface. High density positive interface net charge can be detrimental to the operation of a multi-channel *n-on-p* sensor since the inversion layer generated under the Si/SiO₂-interface can cause loss of position resolution by creating a conduction channel between the electrodes. In the investigation of the radiation-induced accumulation of oxide charge and interface traps, a capacitance-voltage characterization study of *n*/ γ - and γ -irradiated Metal-Oxide-Semiconductor (MOS) capacitors showed that close agreement between measurement and simulation were possible when oxide charge density was complemented by both acceptor- and donor-type deep interface traps with densities comparable to the oxide charges. Corresponding inter-strip resistance simulations of a *n-on-p* sensor with the tuned oxide charge density and interface traps show close agreement with experimental results. The beneficial impact of radiation-induced accumulation of deep interface traps on inter-electrode isolation may be considered in the optimization of the processing parameters of isolation implants on *n-on-p* sensors for the extreme radiation environments.

*Corresponding author

Email address: timo.peltola@ttu.edu (T. Peltola)

1. Introduction

In the high-radiation environment of LHC experiments, where silicon particle detectors are utilized, radiation-induced defects are introduced both in the silicon substrate (bulk damage or displacement damage) and in the SiO₂ passivation layer, that affect the sensor performance through the interface with the Si-bulk (surface damage). An accompanying study to the investigation presented here focused on the influence of displacement damage on the bulk properties of test-diode samples exposed to a reactor radiation environment [1]. In this study, the influence and accumulation of surface damage is investigated by the characterizations of Metal-Oxide-Semiconductor (MOS) capacitors, exposed to either the same reactor radiation environment as in the previous study or to a γ -source.

Surface damage caused by ionizing radiation from charged particles, X-rays or gammas in SiO₂ passivated devices consists of the accumulation of positively charged layer (fixed oxide charge density N_f that does not move or exchange charge with Si), trapped-oxide-charge and interface traps (or surface states N_{it}), along with mobile-ionic-charge density (N_M) inside the oxide and close to the interface with silicon bulk. When exposed to high-energy ionizing radiation, electron-hole pairs are created in the oxide. The fraction of electrons and holes escaping from the initial recombination drift through the oxide either to the gate-electrode or to the Si/SiO₂-interface, depending on the gate bias. Holes transport with positive gate bias through the oxide toward the Si/SiO₂-interface by hopping through localized states in the oxide, and a fraction of the holes that reach the vicinity of the interface are captured by oxygen vacancies (most of the vacancies in the SiO₂ are located close to the Si/SiO₂-interface) and form positive oxide-trapped charge. During the transport of holes, some react with hydrogenated oxygen vacancies and result in protons (hydrogen ions). The fraction of protons that drift to the interface produce dangling Si-bonds, i.e. interface traps, by breaking the hydrogenated Si-bonds at the interface. The mechanisms by which surface damage accumulation occurs are described extensively in [2, 3, 4, 5, 6].

High positive N_f is detrimental to the functionality of segmented *n-on-p* (*p*-bulk with n^+ electrode implants) sensors, since the electron layer generated under the Si/SiO₂-interface can cause loss of position resolution by providing a conduction channel that compromises the inter-electrode isolation. Additionally, the accumulating interface charges can contribute to higher channel noise by the increase of inter-electrode capacitance (C_{int}) and modify the electric fields at the edges of the isolation- and channel-implants. N_{it} can also play a notable role in determining the surface properties of Si-sensors as significant fraction of these interface states have been reported to be deep traps with densities comparable to N_f [7, 8] in X-ray irradiated devices, thus capable of altering the space charge near the Si/SiO₂-interface.

Table 1: An overview of surface damage models complementing N_f with acceptor- ($N_{it,acc}$) and/or donor-type ($N_{it,don}$) N_{it} at the Si/SiO₂-interface. $E_{a,v,c}$ are the activation energy, valence band and conduction band energies, respectively, while V_{fb} , R_{int} and s_0 are the flat-band voltage, inter-strip resistance and surface generation velocity, respectively.

N_{it} type	E_a [eV]	Tuning properties	Reference
Deep acceptor	$E_C - 0.60$	V_{fb} and R_{int}	[12]
Shallow acceptor	$E_C - 0.39$		
Deep donor	$E_V + 0.60$	V_{fb} and s_0	[13, 14]
Deep acceptor	$E_C - 0.56$		
Deep donor	$E_V + 0.70$	R_{int}	[15]
Deep acceptor	$E_C - 0.60$		
Shallow acceptor	$E_C - 0.40$		

Device simulations play a vital role in understanding and parametrizing the observed macroscopic effects of the microscopic surface states and charges at the Si/SiO₂-interface. Previous simulation studies to model the radiation-induced accumulation of surface damage involve several approaches, of which one is to approximate the surface damage solely by N_f (for the modeling of inter-strip resistance (R_{int}) in Ref. [9], C_{int} in Ref. [10] and electric field surface distribution in Ref. [11]). Models complementing N_f with interface traps include approaches presented in Table 1. A further model, tuned to reproduce the charge-injection position dependence of charge collection efficiency (CCE(x)) in the inter-strip region and C_{int} , includes an approach where two bulk defect levels tuned for proton irradiation [16] are augmented by a shallow ($E_C - 0.40$ eV) $N_{it,acc}$ with 2 μm depth distribution from the surface [17, 18].

It needs to be pointed out that for higher tunability of the models the use of a single set of effective interface traps is an approximation of the real situation, where there can be a continuum of levels at the interface.

The approach taken in this study is to first tune N_f and the parameters of N_{it} (number of N_{it} , type, energy level, trapping cross-sections and density) to reproduce CV -characteristics of irradiated MOS-capacitors and next, as a confidence level test of the tuning, monitor their possible influence on the R_{int} of a n -on- p strip-sensor. The inter-strip isolation results are further examined for the dynamical influence of the fully occupied N_{it} on the net N_{ox} in the operating conditions of reverse biased n -on- p sensors.

The paper is arranged by first introducing the samples, the neutron fluences and the γ -doses the samples

were exposed to in Section 2. Next, the measurement and simulation setups are described in Section 3. *CV*-characterization results start with the analysis of pre-irradiated reference MOS-capacitors diced from 6-inch wafers in Section 4.1, where the extracted oxide thicknesses (t_{ox}) and oxide charge densities at the Si/SiO₂-interface (N_{ox0}) are presented. Results of both reactor neutron and γ -irradiated MOS-capacitors are presented in Section 4.2 by first determining the change in the flat band voltage (ΔV_{fb}) after irradiation, followed by the extraction of effective oxide charge density (N_{ox}) at the Si/SiO₂-interface. Technology Computer-Aided Design (TCAD) simulations are applied in both results sections to reproduce and model the measured *CV*-characteristics. The inter-strip resistance simulations applying N_{f} and surface states tuned to reproduce the irradiated MOS-capacitor *CV*-characteristics are presented in the second part of Section 4.2. Finally, the results are discussed in Section 5, while summary and conclusions are given in Section 6.

2. Samples, effective neutron fluences and doses

Out of five reactor irradiated samples in this study, three were irradiated at Rhode Island Nuclear Science Center¹ (RINSC) and two at UC Davis McClellan Nuclear Research Center² (MNRC). Total Ionizing Dose (TID) in both reactor cores was from a mixed field of neutrons and gammas, while the contribution from gammas was expected to dominate TID. Monte Carlo N-Particle Transport (MCNP) simulations indicated that neutron contribution to TID was only about 5% at MNRC. In addition, three samples were γ -irradiated at Sandia National Laboratories Gamma Irradiation Facility³ (GIF) with a ⁶⁰Co-source. After irradiations, the samples were shipped cooled in thermally isolated containers to Texas Tech University (TTU) to avoid annealing of the radiation-induced defects and were then stored at -40° C between the measurements.

Samples like one shown in Figure 1 were diced from 6-inch Hamamatsu Photonics K.K. (HPK) sensor-wafers with $\langle 100 \rangle$ crystal orientation. The test structures on the samples were designed at Institut für Hochenergiephysik (HEPHY). Two distinct diffusion processes were applied in the samples with MOS-capacitors to produce the heavily-doped backplane blocking contact: standard-diffusion ('std-FZ') to produce 300- μm active thickness sensors and deep-diffusion ('dd-FZ') for 200- and 120- μm active thicknesses, while the physical thickness of all samples was 320 μm . Sample identification of e.g. '300P_std-FZ' in Table 2, refers to a 300- μm -active thickness MOS-capacitor with *p*-type float-zone Si-bulk and standard-diffused backplane

¹<http://www.rinsc.ri.gov/>

²<https://mnrc.ucdavis.edu/>

³<https://www.sandia.gov/research/gamma-irradiation-facility-and-low-dose-rate-irradiation-facility/>



Figure 1: Half-moon samples with test structures, diced from a 6-inch Si-wafer. The sample has three test diodes, two MOS-capacitors (second and third from left) and other test structures. The small and large MOS gate areas are $2.5 \times 2.5 \text{ mm}^2$ and $4.0 \times 4.0 \text{ mm}^2$, respectively.

Table 2: Identification of irradiated samples, respective irradiation sites, effective neutron fluences (Φ_{eff}) at RINSC and MNRC, γ -doses at GIF and MCNP-simulated TID at MNRC. N1(n): Lowest fluence reactor-irradiated sample with n -type bulk before irradiation, G2(p): Second to lowest dose γ -irradiated sample with p -type bulk. Bulk material is indicated as 'std-' and 'dd-FZ' that correspond to standard- and deep-diffused float zone substrates, respectively.

Sample ID, thickness & type	Irradiation site	Φ_{eff} [$\times 10^{15} \text{ n}_{\text{eq}} \text{cm}^{-2}$]	D [kGy]	MCNP TID [kGy]
N1(n): 300N_std-FZ	RINSC	0.35 ± 0.04	–	–
N2(n): 300N_std-FZ	MNRC	0.61 ± 0.05	–	7.1 ± 0.6
N3(n): 120N_dd-FZ	RINSC	2.35 ± 0.19	–	–
N4(p): 120P_dd-FZ	RINSC	6.6 ± 0.7	–	–
N5(n): 120N_dd-FZ	MNRC	9.3 ± 1.1	–	90 ± 11
G1(n): 200N_dd-FZ	GIF	–	7.0 ± 0.4	–
G2(p): 300P_std-FZ	GIF	–	23.0 ± 1.2	–
G3(n): 300N_std-FZ	GIF	–	90 ± 5	–

implant. Gate oxide in all samples was silicon dioxide (SiO_2) with positive oxide charge. The corresponding effective 1-MeV neutron equivalent fluences (Φ_{eff}) extracted from the test-diode leakage currents in the samples, γ -doses and MCNP-simulated TIDs are also presented in Table 2. Details of the effective fluence extraction and the bulk properties of the samples are given in [1].

3. Measurement and simulation setups

The capacitance-voltage (CV) characterizations were carried out with a dark-box-enclosed custom probe station at TTU. The gate voltage of the MOS-capacitor is supplied by a Keithley 2410 SMU while the capacitance is read out by a Keysight E4980AL LCR-meter. The decoupling of the LCR-meter's high- and

low-terminals from the DC-circuit is accomplished by 1- μ F capacitors. The remote control and data acquisition functions are carried out with LabVIEW™-based software. The MOS-capacitor is connected to the measurement circuit by a vacuum chuck from its backplane, which also provides fixed position, and by a probe needle on the segmented front surface.

Simulations were carried out using the Synopsys Sentaurus⁴ finite-element TCAD software framework. The parameters extracted from *CV*-measurements of the MOS-capacitors (oxide thickness (t_{ox}), flat band capacitance (C_{fb}) and voltage (V_{fb})) and test diodes on the same samples (bulk doping (N_{B}) and backplane deep-diffusion doping profiles (see ref. [1] for details)) before irradiation, as well as their known gate area, were used as inputs to reproduce the devices as closely as possible by a 2D-simulation.

4. Experimental and simulation results

4.1. Results before irradiation

The *CV*-measurements of six reference MOS-capacitors were carried out at room temperature and the resulting *CV*-characteristics are presented in Figure 2a, where the three modes of operation –accumulation, depletion and inversion– are visible. At gate voltages with $C/C_{\text{ox}} = 1$, where C_{ox} is the oxide capacitance, the majority carriers (holes for *p*-bulk, electrons for *n*-bulk) are pulled to the Si/SiO₂-interface, forming an accumulation layer with zero surface potential. An abrupt drop of capacitance takes place in the depletion region, where the Si-surface is being depleted from majority carriers and measured C is now C_{ox} and depletion layer capacitance in series. Thus, the measured C keeps decreasing with gate voltage as the effective thickness of the depletion region, that acts as a dielectric between the gate and the Si-substrate, increases. Depth of the depletion region reaches its maximum, and measured C its minimum (C_{min}), when most of the available minority carriers are pulled to the Si/SiO₂-interface (by the positive oxide charge and by the negative gate voltage for *p*- and *n*-bulk MOS-capacitors, respectively, in Figure 2a), forming an inversion layer. The depletion region in the measured *CV*-curve is limited by the threshold voltage (V_{th}), where the surface potential equals twice the bulk potential, and the flat band voltage (V_{fb}), where the Si energy band becomes flat and the surface potential goes to zero [2].

Oxide thicknesses were extracted by the relation

$$t_{\text{ox}} = \epsilon_{\text{ox}} \frac{A}{C_{\text{ox}}}, \quad (1)$$

⁴<http://www.synopsys.com>

where ϵ_{ox} is the product of vacuum permittivity and the relative permittivity of the oxide material (SiO_2), and A is the MOS gate area [19]. Flat band voltages were determined by the flat-band-capacitance method with

$$C_{\text{fb}} = \frac{C_{\text{ox}}\epsilon_{\text{S}}A/\lambda}{C_{\text{ox}} + \epsilon_{\text{S}}A/\lambda}, \quad (2)$$

where ϵ_{S} is the permittivity of the substrate material (Si) and λ is the extrinsic Debye length [2]. Flat band voltage V_{fb} is extracted from the CV -curve at the value of C_{fb} . Effective oxide charge densities at the Si/SiO₂-interface were then calculated by

$$N_{\text{ox}} = \frac{C_{\text{ox}}}{eA}(W_{\text{MS}} - V_{\text{fb}}), \quad (3)$$

where W_{MS} is the metal-semiconductor work function and e is the elementary charge. The results for t_{ox} , $V_{\text{fb}0}$ and $N_{\text{ox}0}$ of the reference MOS-capacitors are presented in Table 3. N_{ox} extracted from CV -measurements can be stated as

$$N_{\text{ox}} = N_{\text{f}} + N_{\text{it}} + N_{\text{M}}, \quad (4)$$

where the total value of N_{ox} is influenced by fixed-oxide-charge (N_{f}), interface-trapped-charge (N_{it}) and mobile-ionic-charge (N_{M}) densities [2]. N_{M} can be observed in CV -curve hysteresis when the charges (typically alkali metal ions such as Na^+ , K^+ and Li^+ before irradiation [20]) drift between metal/SiO₂- and Si/SiO₂-interfaces under the applied electric field, depending on the gate bias and the polarity of the charges [2, 21]. The results in Figure 2b do not show any sign of hysteresis. Scanned frequencies involved 1–200 kHz, while the low mobility of N_{M} in oxide (highest for Na^+ with $\mu \approx 4 \times 10^{-12} \text{ cm}^2/\text{Vs}$ at room temperature [2]) that results in long drift time from metal- to Si-interface (about 2 min with $E \approx 10^5 \text{ V/cm}$ and $t_{\text{ox}} \approx 700 \text{ nm}$), was taken into account by applying extended gate-voltage hold-time at strong inversion and strong accumulation before CV -sweep, respectively. Thus, the influence of N_{M} in the reference samples is considered negligible, reducing Eq. 4 to $N_{\text{ox}} \cong N_{\text{f}} + N_{\text{it}}$. This is in contrast with previous results for thin (<25 nm) SiO₂ films, where significant influence of N_{M} was observed [21]. The oxide films in Table 3 –produced by high-growth-rate deposition method like wet thermal oxidation [22, 23]– are about 30 times thicker than the oxide films in ref. [21]. Increased trapping probability of ions with substantially longer drift distance from metal- to Si-interface could explain the lack of influence from N_{M} in the results.

The measured CV -characteristics in Figure 2c were closely reproduced by TCAD simulation. Matching V_{fb} -values within uncertainty to the measured were reached in the simulation by using N_{f} (implemented as a positive charge-sheet located at the Si/SiO₂-interface with a uniform distribution along the interface) as the sole tuning parameter. Frequency-scan $f = 1 - 200 \text{ kHz}$ showed no frequency dependence on the measured

Table 3: Reference sample identification, measured oxide thicknesses (t_{ox}), flat band voltages (V_{fb0}) and the effective oxide charge densities (N_{ox0}) at the Si/SiO₂-interface before irradiation.

Sample thickness & type	t_{ox} [nm]	V_{fb0} [-V]	N_{ox0} [$\times 10^{10} \text{ cm}^{-2}$]
120P_dd-FZ	695 ± 5	4.38 ± 0.03	11.20 ± 0.12
120P_dd-FZ(b)	687 ± 5	5.35 ± 0.04	14.30 ± 0.14
300P_std-FZ	795 ± 4	4.24 ± 0.02	9.39 ± 0.06
200N_dd-FZ	741 ± 16	2.69 ± 0.06	5.59 ± 0.17
300N_std-FZ	749 ± 2	2.750 ± 0.007	6.67 ± 0.02
300N_std-FZ(b)	704 ± 4	2.600 ± 0.015	6.54 ± 0.05

value of V_{fb} , which was repeated by the simulation. The values of N_{ox} (extracted from the measurement) and N_{f} (required in the simulation) for 120P MOS-capacitor in Figure 2c were $(1.120 \pm 0.012) \times 10^{11} \text{ cm}^{-2}$ and $(1.14 \pm 0.02) \times 10^{11} \text{ cm}^{-2}$, respectively, while the corresponding values for 300N were $(6.67 \pm 0.02) \times 10^{10} \text{ cm}^{-2}$ and $(7.00 \pm 0.03) \times 10^{10} \text{ cm}^{-2}$, respectively. In four measured and simulated reference MOS-capacitors the required N_{f} deviated from the measured N_{ox} by $+2.8 \pm 1.5\%$.

Thus, the combined hysteresis and simulation results show evidence that N_{ox} in the reference samples is essentially governed by N_{f} , i.e. $N_{\text{ox}} \cong N_{\text{f}}$. This is in line with the results of ref. [24], where it was reported that N_{it} at the Si/SiO₂-interface of a non-irradiated silicon device is about two-orders-of-magnitude lower than N_{f} at the interface. Therefore, the density of surface traps corresponding to $N_{\text{f}} = 1 \times 10^{11} \text{ cm}^{-2}$ should be in the order of 10^9 cm^{-2} . Additional simulation with surface-trapping-center energy of $E_{\text{a}} = E_{\text{c}} - 0.60 \text{ eV}$ [25, 26] and a fairly large capture cross-section of $1 \times 10^{-14} \text{ cm}^2$ results in identical CV -characteristics to the simulations in Figure 2c until the difference between N_{it} and N_{f} is less than one-order-of-magnitude.

4.2. Results after n/ γ - and γ -irradiations

The CV -measurements of five n/ γ -irradiated and three γ -irradiated MOS-capacitors were carried out at room temperature with frequencies 1–9 kHz, and the resulting CV -characteristics are presented in Figures 3–5. Due to the extended depletion-regions and the gradual change from depletion to accumulation in the CV -curves, most probable estimates for the V_{fb} of the irradiated samples were extracted by both C_{fb} -method in Eq. 2 and from the crossing-point of linear fits to the dynamic (depletion) and static (accumulation) regions of the reciprocal C^2 -curve, as shown in Figure 3a. The final value and the uncertainty of V_{fb} was then given

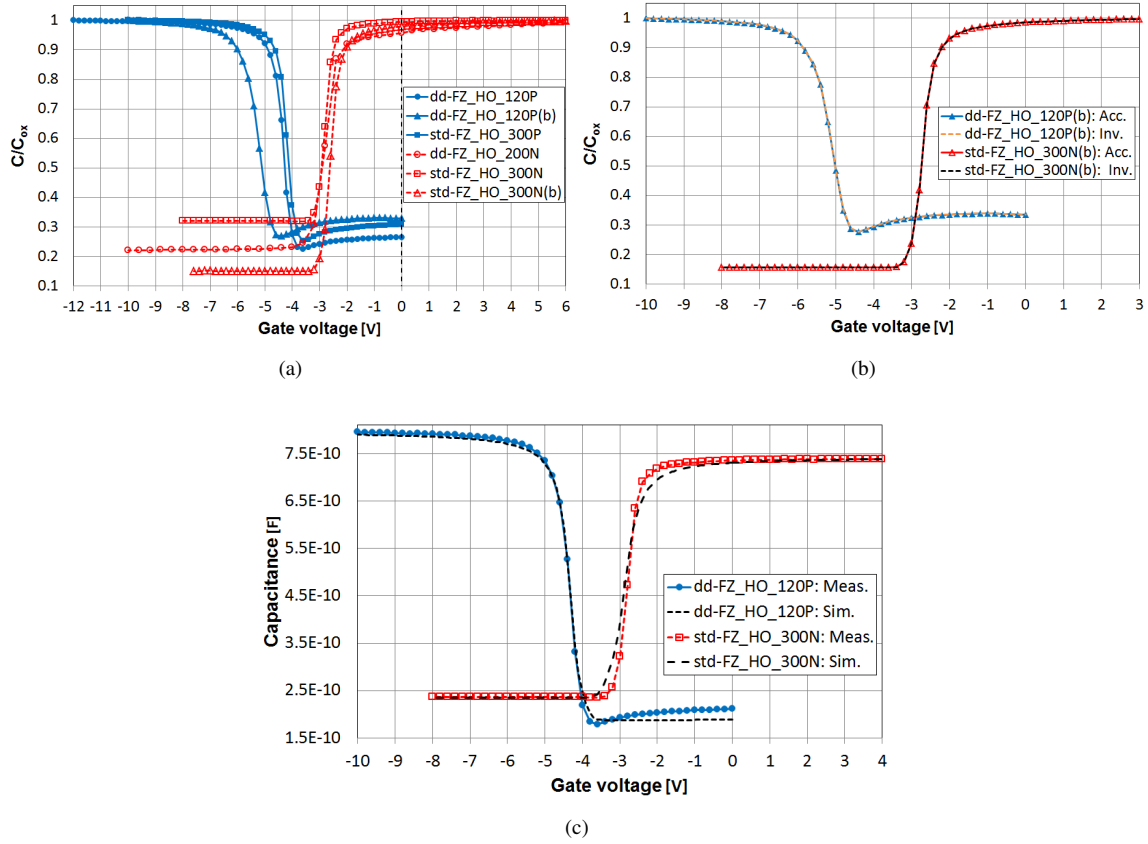


Figure 2: (a) Measured C_{ox} -normalized CV -characteristics of six pre-irradiated reference MOS-capacitors with both p - and n -type bulk materials. (b) Measured C_{ox} -normalized CV -characteristics of p - and n -bulk reference MOS-capacitors with CV -sweep starting either from accumulation (Acc.) or inversion (Inv.) regions. (c) Measured and simulated CV -characteristics of p - and n -bulk reference MOS-capacitors at $T = 293$ K and $f = 200$ kHz.

by the average and the difference of the two extracted values, respectively. The results for V_{fb} and its relative change before and after irradiation (ΔV_{fb}) are presented in Table 4.

The change of N_{ox} with ionizing radiation is proportional to the change of W_{MS} and V_{fb} in Eq. 3 before (W_{MS0} and V_{fb0}) and after irradiation

$$N_{ox} - N_{ox0} = \frac{C_{ox}}{eA}(W_{MS} - W_{MS0} - (V_{fb} - V_{fb0})). \quad (5)$$

The results of the bulk properties of the same reactor-irradiated samples in the accompanying study [1] indicate that the effective bulk doping (N_{eff}) varies in the studied fluence range from a few times 10^{12} cm^{-3} (before irradiation) to close to $1 \times 10^{14} \text{ cm}^{-3}$ (at the highest fluence of about $1 \times 10^{16} \text{ n}_{eq}\text{cm}^{-2}$). The N_{eff} dependence of W_{MS} leads in this range to the maximal change of $\Delta W_{MS,max} \approx 0.12 \text{ V}$, regardless of bulk polarity [2]. In comparison, the values of ΔV_{fb} in Table 4 are two-orders-of-magnitude higher to $\Delta W_{MS,max}$. Thus, contribution from ΔW_{MS} to N_{ox} is considered negligible in the following analysis, simplifying Eq. 5 to

$$N_{ox} \cong \frac{C_{ox}}{eA}(V_{fb0} - V_{fb}) + N_{ox0} = \frac{C_{ox}}{eA}\Delta V_{fb} + N_{ox0}. \quad (6)$$

Since the absolute values of C_{ox} in the n/γ -irradiated MOS-capacitors were observed to fluctuate significantly from the initial C_{ox} before irradiation, the relation applied to extract N_{ox} was reached by combining Eqs. 1 and 6:

$$N_{ox} \cong \frac{\epsilon_{ox}}{t_{ox}e}\Delta V_{fb} + N_{ox0}, \quad (7)$$

where N_{ox} is solely dependent on oxide thickness, change in the flat band voltage and the initial oxide charge density at Si/SiO₂-interface before irradiation. The results for N_{ox} are included in Table 4.

As displayed by the measurements in Figures 3a, 3b, 4a, 5 and 6a, CV -characteristics of the n/γ -irradiated MOS-capacitors are distinctly different compared to the results observed before irradiation. The about 1 V-wide depletion regions displayed in Figure 2 have increased to tens of V and V_{fb} has an opposite sign compared to V_{th} , while hysteresis between CV -sweeps starting either from accumulation or inversion regions is absent. Additionally, the inversion region has a non-zero slope that is independent of measurement and delay times, and of CV -sweep direction, while the accumulation region in the initially n -bulk MOSs has been reversed to opposite sign gate-voltages (V_{gate}) from Figure 2, indicating neutron-irradiation-induced space charge sign inversion (SCSI), where n -type Si-bulk is turned effectively to p -type by the introduction of acceptor-type bulk defects, switching the majority carriers from electrons to holes. Further signs of the neutron-irradiation-induced displacement damage in the Si-substrate is displayed by the significant increase in the ratio C_{min}/C_{ox} [27, 28] (from ≤ 0.3 before irradiation to ≤ 0.83 after irradiation, increasing with fluence). The accumulation

Table 4: Identification of the irradiated samples, total ionizing doses (TID), measured flat band voltages (V_{fb}), relative change in V_{fb} before and after irradiation (ΔV_{fb}) and Si/SiO₂-interface oxide charge densities (N_{ox}) after irradiation. Corresponding CV -sweep starting regions for inversion (Inv.) and accumulation (Acc.) are also indicated. The TID-values in parentheses are interpolations from MCNP-simulated TIDs.

Sample ID	TID [kGy]	CV -sweep	V_{fb} [-V]	ΔV_{fb} [V]	N_{ox} [$\times 10^{12} \text{ cm}^{-2}$]
N1(n)	–	Inv./Acc.	22.7 ± 1.5	20.0 ± 1.3	0.64 ± 0.04
N2(n)	7.1 ± 0.6	Inv./Acc.	26 ± 3	23 ± 3	0.77 ± 0.10
N3(n)	(23.5 ± 1.9)	Inv./Acc.	37 ± 4	34 ± 3	1.06 ± 0.15
N4(p)	(64 ± 7)	Inv./Acc.	65 ± 4	59 ± 4	2.00 ± 0.14
N5(n)	90 ± 11	Inv./Acc.	71 ± 6	68 ± 6	2.1 ± 0.3
G1(n)	7.0 ± 0.4	Inv.	86 ± 4	83 ± 4	2.47 ± 0.15
		Acc.	76 ± 4	73 ± 4	2.19 ± 0.14
G2(p)	23.0 ± 1.2	Inv.	62 ± 7	58 ± 7	1.66 ± 0.19
		Acc.	81 ± 8	77 ± 7	2.17 ± 0.20
G3(n)	90 ± 5	Inv.	111 ± 14	108 ± 14	3.2 ± 0.4
		Acc.	85 ± 13	82 ± 12	2.4 ± 0.4

of displacement damage with neutron irradiation in the Si-bulk of the samples is considered only qualitatively in the scope of this study, while more detailed investigation is presented in [1]. Finally, to produce stable CV -curves from the n/γ -irradiated MOSs, careful tuning of the measurement frequency was required, resulting in specific f (1–9 kHz) for each of the five investigated fluences. The three γ -irradiated MOS-capacitors in the study were exposed to doses within uncertainty to the corresponding TID-values of the three neutron irradiated MOSs in Table 4, and were measured at identical frequencies to the n/γ -irradiated MOSs to enable meaningful comparison.

Although the threshold energy for X-rays or gammas to induce bulk damage has been reported to be about 300 keV [6] ($E_{\gamma}({}^{60}\text{Co}) = 1.173, 1.332 \text{ MeV}$), none of the aforementioned bulk damage effects are visible on the CV -characteristics of the MOS-capacitors irradiated solely by gammas in Figures 3c, 4b and 6b. The depletion region has again expanded to tens of V, as for n/γ -irradiated MOSs, but V_{th} and V_{fb} are now of the same sign, while the CV -curves starting from the accumulation or inversion regions display significant hysteresis ($\geq 10 \text{ V}$) that increases with dose. In Figures 3c, 4b and 6b higher absolute value of V_{fb} (= higher

positive N_{ox}) is always seen when CV -sweep starts from negative V_{gate} . This rules out the influence of N_{M} , that at negative V_{gate} would always reduce the net value of positive N_{ox} , regardless of the charge sign of N_{M} .

The comparison between the γ -irradiated MOS-capacitors with doses within uncertainty to the corresponding MCNP-simulated/interpolated TID-values of the three n/γ -irradiated MOSs in Table 4 shows systematically lower V_{fb} and N_{ox} -values for the n/γ -irradiated MOSs, suggesting that the simulated TID-levels at MNRC reactor were overestimated.

To investigate and reproduce the CV -characteristics of the irradiated MOS-capacitors in Figures 3–6 by TCAD simulation, MOS-structures with input parameters described in Section 3 were applied. For the n/γ -irradiated MOSs, the occurrence of SCSi in n -type bulk and the accumulation of the effective bulk doping with neutron fluence were approximated by using p -type bulk and tuning N_{eff} to reach similar $C_{\text{min}}/C_{\text{ox}}$ -ratios with the measurements, while for γ -irradiated MOSs, in the absence of displacement damage in the bulk, both n - and p -bulks were utilized. Simulations were carried out at matching temperature and frequencies to the measurements.

As shown in Figures 3c and 4a, including only N_{f} (within uncertainty to the measured N_{ox} in Table 5) at the Si/SiO₂-interface results in an abrupt depletion region that does not reproduce the characteristics of the measured CV -curves of either n/γ - or γ -irradiated MOS-capacitors. Hence, close agreement between measured and simulated CV -characteristics was found to require the introduction of both donor- and acceptor-type N_{it} ($N_{\text{it,don}}$ and $N_{\text{it,acc}}$, respectively) at the interface. Data from previous studies on X-ray irradiated MOS-capacitors and strip sensors [6, 8, 24, 25, 29, 30, 31] was used as a starting point for setting the parameter values of N_{it} in Table 6, and for further tuning, the surface-state dynamics [2],

$$\begin{aligned}
&N_{\text{f}} : \text{always fully occupied,} \\
&\text{unoccupied } N_{\text{it,don}} \ \& \ N_{\text{it,acc}} : Q_{\text{it}} = 0, \\
&\text{fully occupied } N_{\text{it,don}} : Q_{\text{it}} = +e, \ \text{and} \\
&\text{fully occupied } N_{\text{it,acc}} : Q_{\text{it}} = -e,
\end{aligned} \tag{8}$$

where Q_{it} is the interface-trapped charge and e is the elementary charge, were considered.

The fully occupied $N_{\text{it,acc}}$ increase the electron density at the Si/SiO₂-interface, reducing the net positive oxide charge at the interface, eventually moving V_{th} from negative to positive V_{gate} with the tuned parameter values presented in Tables 5 and 6. The fully occupied $N_{\text{it,don}}$ keep the hole density at the interface high enough to widen the depletion region over an extended voltage range with a gradual slope. After the tuning of the parameter values for agreeing CV -characteristics with the measurements, the densities of both types

Table 5: Irradiated sample identification, CV -sweep starting regions for inversion (Inv.) and accumulation (Acc.), measured Si/SiO₂-interface oxide charge densities (N_{ox}) after irradiation, and TCAD-simulation input densities for fixed oxide charge (N_f) and donor- and acceptor-type interface traps ($N_{\text{it,don}}$ & $N_{\text{it,acc}}$, respectively) from Table 6 to reproduce measured CV -characteristics in Figures 3–6.

Sample ID	CV -sweep	N_{ox} [$\times 10^{12} \text{ cm}^{-2}$]	TCAD N_f [$\times 10^{12} \text{ cm}^{-2}$]	TCAD $N_{\text{it,don}}$ [$\times 10^{12} \text{ cm}^{-2}$]	TCAD $N_{\text{it,acc}}$ [$\times 10^{12} \text{ cm}^{-2}$]
N1(n)	Inv./Acc.	0.64 ± 0.04	0.68	1.11	1.08
N2(n)	Inv./Acc.	0.77 ± 0.10	0.77	1.65	1.59
N3(n)	Inv./Acc.	1.06 ± 0.15	1.00	2.30	2.60
N4(p)	Inv./Acc.	2.00 ± 0.14	1.75	3.25	4.70
N5(n)	Inv./Acc.	2.1 ± 0.3	2.20	4.15	4.35
G1(n)	Inv.	2.47 ± 0.15	0.79	1.92	1.10
	Acc.	2.19 ± 0.14	0.79	1.65	1.10
G2(p)	Inv.	1.66 ± 0.19	1.20	1.70	1.15
	Acc.	2.17 ± 0.20	1.20	2.11	1.00
G3(n)	Inv.	3.2 ± 0.4	2.20	1.05	1.50
	Acc.	2.4 ± 0.4	2.00	0.50	1.00

Table 6: The simulation input parameters of radiation-induced N_{it} . $E_{a,v,c}$ are the activation energy, valence band and conduction band energies, respectively, while $\sigma_{e,h}$ are the electron and hole trapping cross sections, respectively.

N_{it} type	E_a [eV]	$\sigma_{e,h}$ [cm ²]	Density [cm ⁻²]
Deep donor ($N_{\text{it,don}}$)	$E_V + 0.65$	1×10^{-15}	see column 5 in Table 5
Deep acceptor ($N_{\text{it,acc}}$)	$E_C - 0.60$	1×10^{-15}	see column 6 in Table 5

of N_{it} in Table 5 remain comparable to the magnitude of N_f , which is in line with previous experimental observations [7, 8, 12]. Additionally, to reproduce the measured CV -characteristics, it was found to be necessary that both N_{it} are deep traps, since tuning of one or both N_{it} with shallow (0.39 eV and 0.48 eV) traps reported in [29] did not produce agreement with the measurements. Also, the E_a of $N_{\text{it,don}}$ needed to be tuned from the initial $E_V + 0.60$ eV to $E_V + 0.65$ eV in Table 6 for a closer match with the experimental results. The trapping cross-section $1 \times 10^{-15} \text{ cm}^2$ for deep traps in [29] was not tuned from the initial value for both electrons and holes.

For n/γ -irradiated MOS-capacitors, the accuracy of the simulation degrades at the highest positive V_{gate} -

values in Figures 3a, 3b, 4a and 6a, where an increasing number of minority carriers are pulled to the Si/SiO₂-interface. Above V_{th} , the simulated CV -curve stabilizes to a constant value in the inversion region, which is not seen in the measurement. This is due to all $N_{it,don}$ becoming unoccupied, resulting in the net positive interface charge being composed solely of N_f ($N_f = 1.00 \times 10^{12} \text{ cm}^{-2}$ in row three of Table 5), as shown in Figure 7a where simulated interface-trapped charge density is displayed as a function of V_{gate} . Thus, in the absence of N_M , the net oxide charge density can be described as

$$Q_{ox} = eN_{ox} = e[N_f + aN_{it,don} - bN_{it,acc}], \quad (9)$$

where a and b are the fractions of fully occupied $N_{it,don}$ and $N_{it,acc}$, respectively. In Figure 7a, the values of a and b at -100 V are 1.00 and 0.18, respectively, while at +80 V the corresponding values are 0.0 and 1.0, respectively. This effectively makes Q_{ox} in Eq. 9 a dynamic characteristic that experiences polarity change with V_{gate} .

For γ -irradiated MOS in Figure 4b the measured $C > C_{min}$ at deep inversion, showing signs of low-frequency measurement behavior where the inversion-layer charge is supplied/removed quickly enough to respond to changes in V_{gate} (reducing depletion layer depth and increasing inversion C towards C_{ox}) [2], which is not reproduced by the otherwise closely agreeing simulation at $f = 4 \text{ kHz}$. The other visible disagreement between measured and simulated γ -irradiated MOS-capacitors' CV -characteristics is seen in Figure 6b, where the abrupt slope change at about 25 V into depletion-region after V_{th} in measured CV -curve is not reproduced by the simulation. This could be evidence of an additional N_{it} level introduced to the Si/SiO₂-interface at high doses, $N_{it,don}$ and $N_{it,acc}$ for p - and n -bulk MOSs, respectively, that becomes fully occupied at given V_{gate} -value and stops contributing dynamically to the shape of the depletion-region CV -slope.

Using tuned values of N_f , $N_{it,don}$ and $N_{it,acc}$, it is possible to analytically find estimates for a and b in Eq. 9 that produce matching N_{ox} with the measured values in Table 5. By plotting the TCAD-simulated evolution of peak-density-normalized fully occupied $N_{it,don}$ and $N_{it,acc}$, i.e. interface-trapped charge densities, with V_{gate} in Figure 7b, it is possible to directly extract a and b at the point of V_{fb} . For n -bulk MOS G1(n) in Figure 7b $a = 1.00$ and $b = 0.22$, resulting in $N_{ox} = 2.2 \times 10^{12} \text{ cm}^{-2}$ (with N_f , $N_{it,don}$ and $N_{it,acc}$ values for CV -sweep starting from accumulation in Table 5) that is within uncertainty of the measured N_{ox} . Corresponding values of a and b for MOS N2(n) in the same figure are 0.92 for both, resulting in $N_{ox} = 0.825 \times 10^{12} \text{ cm}^{-2}$, which again is within uncertainty of the measured value. Thus, TCAD simulation and Eq. 9 provide a prediction of the fraction of fully occupied $N_{it,don}$ and $N_{it,acc}$ at V_{fb} , where N_{ox} is extracted.

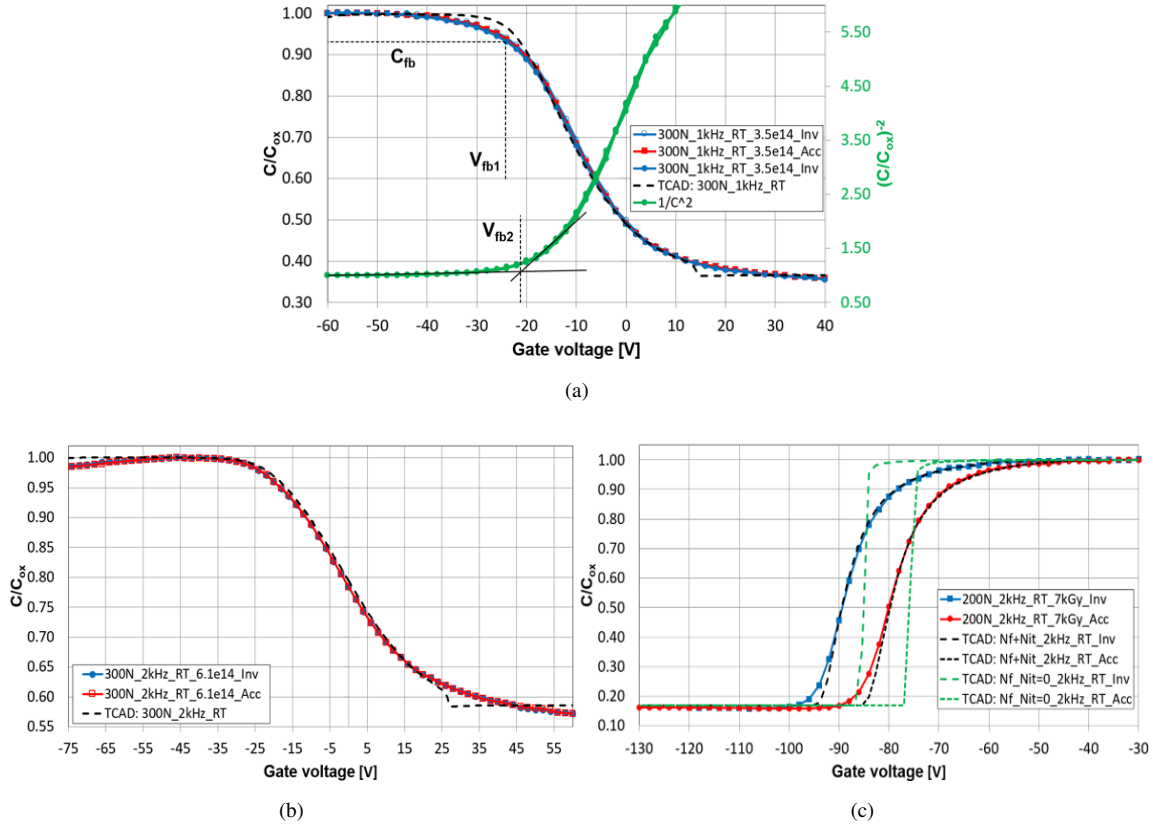


Figure 3: Measured and simulated CV -characteristics at $T = RT$ for a (a) 300- μm -thick initial n -bulk (type inverted to p -bulk) MOS-capacitor (ID: N1(n)) n/γ -irradiated to the fluence of $(3.5 \pm 0.4) \times 10^{14} \text{ n}_{\text{eq}}\text{cm}^{-2}$ and measured at $f = 1 \text{ kHz}$ (with the two methods to extract measured V_{fb} displayed), (b) 300- μm -thick initial n -bulk (type inverted to p -bulk) MOS-capacitor (ID: N2(n)) n/γ -irradiated to the fluence of $(6.1 \pm 0.5) \times 10^{14} \text{ n}_{\text{eq}}\text{cm}^{-2}$ (and to the MCNP-simulated TID = $7.1 \pm 0.6 \text{ kGy}$) and measured at $f = 2 \text{ kHz}$, and (c) 200- μm -thick n -bulk MOS-capacitor (ID: G1(n)) γ -irradiated to the dose of $7.0 \pm 0.4 \text{ kGy}$ and measured at $f = 2 \text{ kHz}$. Measurements included voltage-scans starting from both inversion (Inv.) and accumulation (Acc.) regions. Simulation input parameters in Figures 3–6 are presented in Tables 6 and 5.

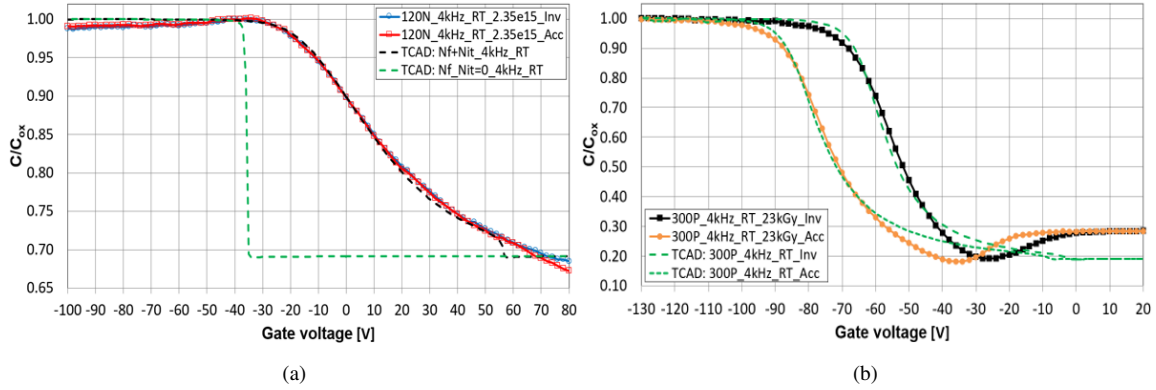


Figure 4: Measured and simulated CV -characteristics at $T = RT$ and $f = 4$ kHz for a (a) 120- μm -thick initial n -bulk (type inverted to p -bulk) MOS-capacitor (ID: N3(n)) n/γ -irradiated to the fluence of $(2.35 \pm 0.19) \times 10^{15} \text{ n}_{\text{eq}}\text{cm}^{-2}$, and (b) 300- μm -thick p -bulk MOS-capacitor (ID: G2(p)) γ -irradiated to the dose of 23.0 ± 1.2 kGy. Measurements included voltage-scans starting from both inversion (Inv.) and accumulation (Acc.) regions.

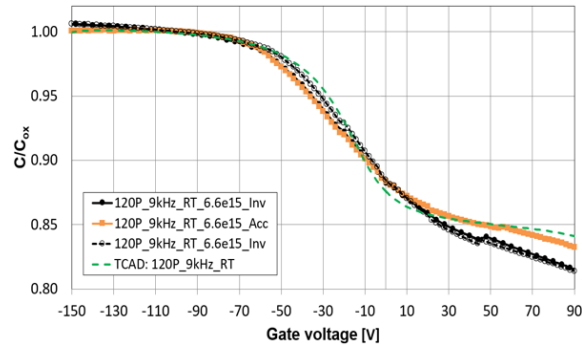


Figure 5: Measured and simulated CV -characteristics at $T = RT$ and $f = 9$ kHz for 120- μm -thick p -bulk MOS-capacitor n/γ -irradiated to the fluence of $(6.6 \pm 0.7) \times 10^{15} \text{ n}_{\text{eq}}\text{cm}^{-2}$ (ID: N4(p)). Measurements included voltage-scans starting from both inversion (Inv.) and accumulation (Acc.) regions.

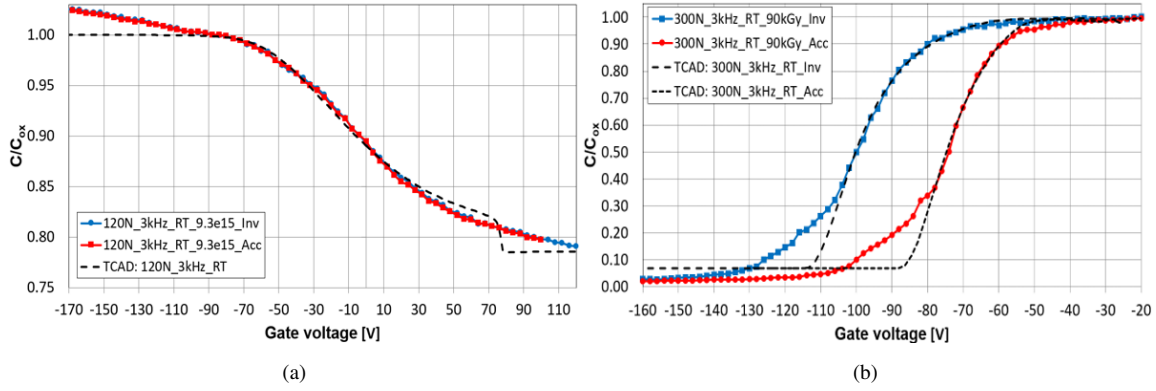


Figure 6: Measured and simulated CV -characteristics at $T = \text{RT}$ and $f = 3 \text{ kHz}$ for a (a) 120- μm -thick initial n -bulk (type inverted to p -bulk) MOS-capacitor (ID: N5(n)) n/γ -irradiated to the fluence of $(9.3 \pm 1.1) \times 10^{15} \text{ n}_{\text{eq}}\text{cm}^{-2}$ (and to the MCNP-simulated TID = $90 \pm 11 \text{ kGy}$), and (b) 300- μm -thick n -bulk MOS-capacitor (ID: G3(n)) γ -irradiated to the dose of $90 \pm 5 \text{ kGy}$. Measurements included voltage-scans starting from both inversion (Inv.) and accumulation (Acc.) regions.

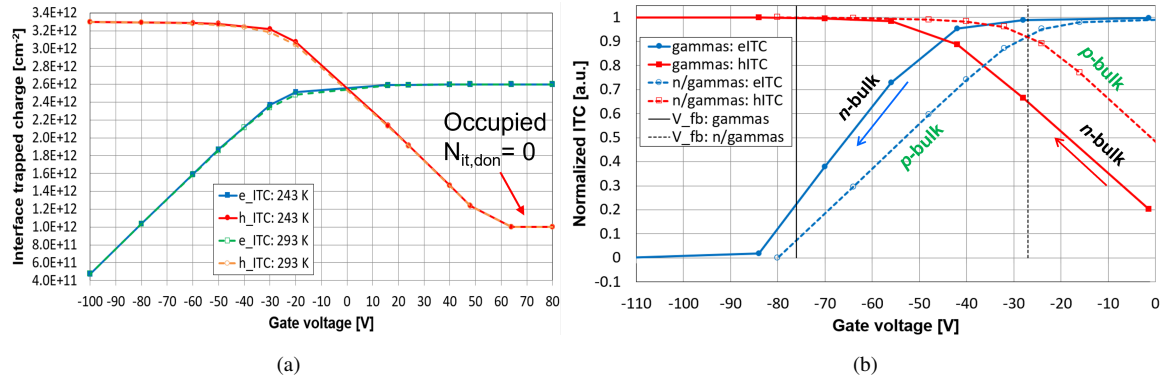


Figure 7: Simulated interface trapped charge densities for (a) a 120- μm -thick p -bulk (type inverted from n -bulk) MOS-capacitor at $T = +20^\circ$ and -30° C , n/γ -irradiated to the fluence of $(2.35 \pm 0.19) \times 10^{15} \text{ n}_{\text{eq}}\text{cm}^{-2}$ (from Figure 4a), and (b) 300- μm -thick p -bulk (type inverted from n -bulk) and 200- μm -thick n -bulk MOS-capacitors at $T = +20^\circ \text{ C}$, n/γ - and γ -irradiated to the fluence of $(6.1 \pm 0.5) \times 10^{14} \text{ n}_{\text{eq}}\text{cm}^{-2}$ (MCNP-simulated TID = $7.1 \pm 0.6 \text{ kGy}$) and dose of $7.0 \pm 0.4 \text{ kGy}$, respectively (from Figures 3b and 3c, respectively). The simulation input parameters of the γ -irradiated MOS correspond to the CV -curves starting from the accumulation-region in Figure 3c.

The V_{gate} -dependent dynamic properties of Q_{ox} in Eq. 9 can potentially lead to improved isolation of segmented electrodes (e.g. pads, strips, pixels) in irradiated n -on- p devices, that are in danger of getting shorted at high levels of positive polarity N_{ox} . This was investigated in Figure 8 by using N_{f} , $N_{\text{it,don}}$ and $N_{\text{it,acc}}$ in Table 5, tuned to the measured CV -characteristics of the MOS-capacitors N3(n) (with $\Phi_{\text{eff}} = (2.35 \pm 0.19) \times 10^{15} \text{ n}_{\text{eq}}\text{cm}^{-2}$) and N5(n) (with $\Phi_{\text{eff}} = (9.3 \pm 1.1) \times 10^{15} \text{ n}_{\text{eq}}\text{cm}^{-2}$) as an input at the Si/SiO₂-interface for an inter-strip resistance (R_{int})-simulation of a n -on- p sensor structure in Figure 8a. Displayed in Figure 8b, high levels of R_{int} (ρ_{int}) are maintained throughout the investigated reverse bias V -range ($V_{\text{bias}} = 0 - 1 \text{ kV}$), for the ‘standard’ value of p -stop peak doping (STD N_{ps}) and regardless of the p -stop configuration. Both the voltage dependence and absolute values of ρ_{int} are in close agreement with previously reported experimental results of X-ray [15] and reactor [32, 33] irradiated strip-sensors, while the gradual decay of measured R_{int} with fluence is also reproduced. By excluding $N_{\text{it,don}}$ and $N_{\text{it,acc}}$ from the simulation, the strips become either shorted (STD N_{ps} , $N_{\text{it}} = 0$ in Figure 8b) for all voltages or reach isolation only above 500 V of V_{bias} for an extreme value of p -stop peak doping ($5 \times \text{STD } N_{\text{ps}}$, $N_{\text{it}} = 0$).

Figure 8c shows the effect of fully occupied N_{it} on N_{ox} in the inter-strip region with the evolution of the positive potential at the strip electrode. For the MOS-capacitor N3(n), after polarity change from negative to positive between 0–10 V the values of N_{ox} at the Si/SiO₂-interface only increase beyond pre-irradiated levels in Table 3 above 700 V, resulting in high R_{int} throughout the V -range. Even though N_{ox} keeps increasing above $2 \times 10^{11} \text{ cm}^{-2}$ (for N3(n) between 0–1 kV a and b in Eq. 9 change from 0.679 and 0.991 to 0.782 and 0.988, respectively), the corresponding ρ_{int} in Figure 8b keeps growing, since electrons are getting increasingly swiped from the inter-strip region to the strip-electrodes at extreme voltages. The decay of R_{int} for the higher fluence N5(n) from the levels observed for N3(n) in Figure 8b, is reflected by the higher values of N_{ox} at $V > 250 \text{ V}$. Hence, the experimentally observed high R_{int} -values in irradiated n -on- p strip-sensors can be explained by the beneficial effect to R_{int} from the radiation-induced accumulation of N_{it} . Similar observations have been reported in previous simulation studies [15, 34] with varied approaches in the application of N_{it} .

5. Discussion

The f -dependence of the irradiated MOS-capacitor CV -characteristics is introduced by the capture and emission rates of N_{it} [2], which is opposite for $N_{\text{it,don}}$ and $N_{\text{it,acc}}$. Thus, at increased f a larger fraction of $N_{\text{it,don}}$ and $N_{\text{it,acc}}$ are fully occupied and unoccupied, respectively, leading to higher positive net oxide charge at Si/SiO₂-interface, while at decreased f the trap occupation is reversed, resulting in lower positive N_{ox}

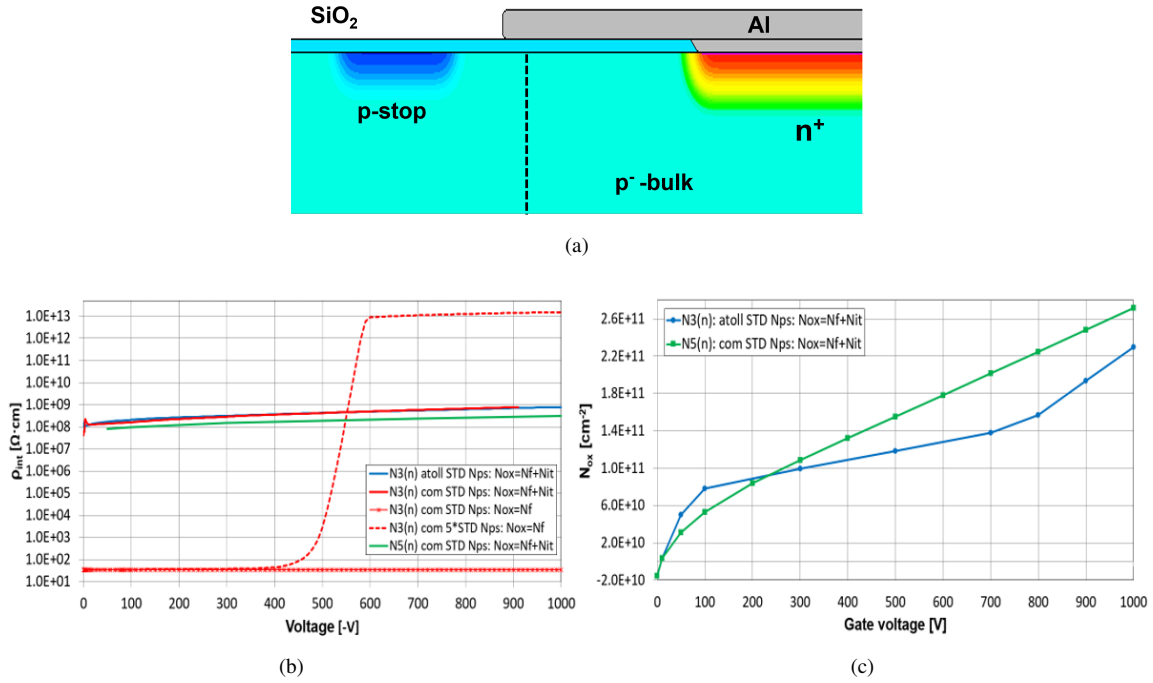


Figure 8: Inter-strip simulations of a 300 μm -thick n -on- p sensor with 50 μm strip-to-strip gap. (a) Close-up of the device structure from midgap to strip-implant with different layers and regions indicated. Dashed black line marks the location of the cut along the device surface in Figure 8c. (b) Inter-strip resistivity evolution with reverse bias voltage at -20°C for individual (atoll) and common p -stop isolation implants ($w_{ps} = 6\ \mu\text{m}$, $d_{ps} = 1.7\ \mu\text{m}$, standard value of p -stop peak doping: STD $N_{ps} = 9 \times 10^{15}\ \text{cm}^{-3}$), simulated by applying N_f and N_{it} -parameters tuned from the measurements and simulations of MOS-capacitors N3(n) ($\Phi_{\text{eff}} = (2.35 \pm 0.19) \times 10^{15}\ \text{neqcm}^{-2}$) and N5(n) ($\Phi_{\text{eff}} = (9.3 \pm 1.1) \times 10^{15}\ \text{neqcm}^{-2}$). (c) N_{ox} evolution with gate (strip) voltage at the Si/SiO₂-interface for the N3(n) with atoll p -stop and N5(n) in Figure 8b.

and therefore lower negative gate voltage produces the flat-band condition in both p - and n -bulk devices. Additionally, the Boltzmann statistics of deep-trap-level e_{it} introduces significant temperature dependence ($e_{it} \propto e^{-E_a/kT}$, where E_a is the activation energy of the trap) [2], when the capture and emission rates slow down with lower T and measurements with constant f result in substantially different V_{fb} and CV -characteristics already within $\pm 20^\circ$ C. These compromise the assessment of any fluence or dose-dependence of the Si/SiO₂-interface properties from MOS CV -characteristics, since the results are only valid for the given measurement f and T . Frequency dependence changes also with the densities of N_{it} , thus no conclusions on the evolution of the oxide-interface properties between n/γ - and γ -irradiated MOS-capacitors or between different fluences and doses are included in this study.

6. Summary and conclusions

Combined experimental and simulation CV -characterization study of MOS-capacitor samples diced from 6-inch wafers –with about 700-nm-thick gate oxides– suggests that N_{ox} at the Si/SiO₂-interface changes from being dominated by N_f before irradiation to include both deep donor- ($E_V + 0.65$ eV) and deep acceptor-type ($E_C - 0.60$ eV) N_{it} , with comparable densities to N_f , after being exposed to either a γ -source or to a reactor radiation environment. This was found by the process of reproducing the measured CV -characteristics of five n/γ -irradiated and three γ -irradiated MOS-capacitors by a TCAD-simulation, where close agreement between measurement and simulation were only reached when in addition to N_f , both $N_{it,don}$ and $N_{it,acc}$ were included in the tuning.

Due to the V_{gate} -dependence of the fraction of the fully occupied $N_{it,don}$ and $N_{it,acc}$, the dynamic nature of N_{ox} can explain the experimentally observed high levels of inter-electrode resistance in irradiated n -on- p devices, like strip-sensors. An R_{int} -simulation of a n -on- p strip-sensor structure using N_f , $N_{it,don}$ and $N_{it,acc}$ (tuned to reproduce the CV -characteristics of an irradiated MOS-capacitor) as an input, showed close agreement for both the voltage dependence and absolute values of R_{int} with previously reported experimental results of X-ray and reactor irradiated strip-sensors. High values of simulated R_{int} were due to the low levels of N_{ox} in the inter-strip region between the strip-anodes.

Thus, the simulation study provides two separate observations of the macroscopic effects of the radiation-induced accumulation of N_{it} at the Si/SiO₂-interface that can explain the experimental results. The N_{it} -accumulation-generated beneficial impact on inter-electrode isolation in irradiated n -on- p sensors suggests that very high levels of p -stop peak doping ($\gtrsim 5 \times 10^{16}$ cm⁻³) could be avoided, mitigating the probability

of discharges or avalanche effects due to excessive electric fields at the p -stops in the extreme radiation environment of the foreseen high-luminosity LHC.

Acknowledgements

This work has been supported by the US Department of Energy, Office of Science (DE-SC0015592). We thank the HGAL and CMS Tracker collaborations of the CMS Experiment for providing the samples investigated in this study. We thank K. Zinsmeyer, C. Perez, and posthumously P. Cruzan of TTU for their expert technical support.

References

- [1] T. Peltola, et al., Charge Collection and Electrical Characterization of Neutron Irradiated Silicon Pad Detectors for the CMS High Granularity Calorimeter, JINST 15 (2020) P09031. doi:10.1088/1748-0221/15/09/P09031.
- [2] E. H. Nicollian, J. R. Brews, MOS (Metal Oxide Semiconductor) Physics and Technology, John Wiley & Sons, New York NY U.S.A., 1982.
- [3] T. P. Ma, P. V. Dressendorfer, Ionizing Radiation Effects in MOS Devices and Circuits, John Wiley & Sons, New York NY U.S.A., 1989.
- [4] T. R. Oldham, Ionizing Radiation Effects in MOS Oxides, World Scientific Publishing, Singapore, 1999.
- [5] J. R. Schwank, et al., Radiation Effects in MOS Oxides, IEEE Trans. Nucl. Sci. 55 (4) (2008) 1833–1853. doi:10.1109/TNS.2008.2001040.
- [6] J. Zhang, et al., Investigation of X-ray induced radiation damage at the Si-SiO₂ interface of silicon sensors for the European XFEL, JINST 7 (2012) C12012. doi:10.1088/1748-0221/7/12/C12012.
- [7] S. Kim, et al., The effects of X-ray irradiation-induced damage on reliability in MOS structures, Solid-State Electronics 38 (1995) 95–99. doi:10.1016/0038-1101(94)E0054-I.
- [8] J. Zhang, X-ray Radiation Damage Studies and Design of a Silicon Pixel Sensor for Science at the XFEL, Ph.D. thesis, University of Hamburg (2013).
URL <https://bib-pubdb1.desy.de/record/152137/files/DESY-2013-00115.pdf>

- [9] G. Verzellese, G.-F. D. Betta, G. Pignatelli, Compact modeling of n-side interstrip resistance in p-stop and p-spray isolated double-sided silicon microstrip detectors, in: 2000 IEEE Nuclear Science Symposium, IEEE, Lyon, France, 2000, pp. 25–27. doi:10.1109/NSSMIC.2000.949004.
- [10] C. Piemonte, Device simulations of isolation techniques for silicon microstrip detectors made on p-type substrates, IEEE Trans. Nucl. Sci NS-53 (2006) 1694–1705. doi:10.1109/TNS.2006.872500.
- [11] Y. Unno, et al., Optimization of surface structures in n-in-p silicon sensors using TCAD simulation, Nucl. Instr. & Meth. A 636 (2011) 118–124. doi:10.1016/j.nima.2010.04.095.
- [12] R. Dalal, et al., Simulation of irradiated Si detectors, PoS 030 (2014) (VERTEX2014). doi:10.22323/1.227.0030.
- [13] A. Morozzi, F. Moscatelli, D. Passeri, G. M. Bilei, TCAD advanced radiation damage modeling in silicon detectors, PoS 050 (2020) (VERTEX2019). doi:10.22323/1.373.0050.
- [14] A. Morozzi, F. Moscatelli, T. Croci, D. Passeri, TCAD Modeling of Surface Radiation Damage Effects: A State-Of-The-Art Review, Front. in Phys. 9 (2021) 617322. doi:10.3389/fphy.2021.617322.
- [15] F. Moscatelli, D. Passeri, A. Morozzi, S. Mattiazzo, G. F. Dalla Betta, M. Dragicevic, G. M. Bilei, Effects of Interface Donor Trap States on Isolation Properties of Detectors Operating at High-Luminosity LHC, IEEE Trans. Nucl. Sci. 64 (8) (2017) 2259–2267. doi:10.1109/TNS.2017.2709815.
- [16] R. Eber, Investigations of new sensor designs and development of an effective radiation damage model for the simulation of highly irradiated silicon particle detectors, Ph.D. thesis, Karlsruhe Institute of Technology (2013).
URL <http://digbib.ubka.uni-karlsruhe.de/volltexte/1000038403>
- [17] T. Peltola, et al., A method to simulate the observed surface properties of proton irradiated silicon strip sensors, JINST 10 (2015) C04025. doi:10.1088/1748-0221/10/04/C04025.
- [18] T. Peltola, Numerical simulations of semiconductor radiation detectors for high-energy physics and spectroscopy applications, Ph.D. thesis, University of Helsinki (2016).
URL <https://helda.helsinki.fi/bitstream/handle/10138/159441/numerica.pdf?sequence=1>

- [19] S. M. Sze, *Physics of Semiconductor Devices*, 2nd Edition, John Wiley & Sons, Hoboken New Jersey U.S.A., 1981.
- [20] G. Greeuw, J. F. Verwey, The mobility of Na⁺, Li⁺, and K⁺ ions in thermally grown SiO₂ films, *J. Appl. Phys.* 56 (8) (1984) 2218–2224. doi:10.1063/1.334256.
- [21] A. J. Suria, H. C. Chiamori, A. Shankar, D. G. Senesky, Capacitance-voltage characteristics of gamma irradiated Al₂O₃, HfO₂, and SiO₂ thin films grown by plasma-enhanced atomic layer deposition, in: *Sensors for Extreme Harsh Environments II*, Vol. 9491, SPIE, 2015, pp. 6 – 13. doi:10.1117/12.2179129.
- [22] P. O. Oviroh, et al., New development of atomic layer deposition: processes, methods and applications, *Sci. Technol. Adv. Mater.* 20 (1) (2019) 465 – 496. doi:10.1080/14686996.2019.1599694.
- [23] R. C. Jaeger, *Introduction to Microelectronic Fabrication*, Vol. 5, in *The Modular Series on Solid State Devices*, 2nd Edition, Addison-Wesley, 2002.
- [24] T. Poehlsen, et al., Charge losses in segmented silicon sensors at the Si-SiO₂ interface, *Nucl. Instr. & Meth. A* 700 (2013) 22–39. doi:10.1016/j.nima.2012.10.063.
- [25] J. Zhang, et al., X-ray induced radiation damage in segmented p⁺n silicon sensors, *PoS 019* (2012) (VERTEX2012). doi:10.22323/1.167.0019.
- [26] T. Peltola, Simulation of radiation-induced defects, *PoS 031* (2015) (VERTEX2015). doi:10.22323/1.254.0031.
- [27] P. Fernández-Martínez, et al., Analysis of displacement damage effects on MOS capacitors, *Nucl. Instr. & Meth. A* 730 (2013) 91–94. doi:10.1016/j.nima.2013.05.108.
- [28] J. A. Luna-López, M. Aceves-Mijares, O. Malik, R. Glaenzer, Modelling the C-V characteristics of MOS capacitor on high resistivity silicon substrate for PIN photodetector applications, *Revista Mexicana de Física* 52 (2) (2006) 45–47.
URL <https://www.researchgate.net/publication/242092497>
- [29] J. Zhang, et al., Study of radiation damage induced by 12 keV X-rays in MOS structures built on high-resistivity *n*-type silicon, *J. Synchrotron Rad.* 19 (2012) 340–346. doi:10.1107/S0909049512002348.

- [30] T. Poehlsen, et al., Study of the accumulation layer and charge losses at the Si-SiO₂ interface in p^+n -silicon strip sensors, Nucl. Instr. & Meth. A 721 (2013) 26–34. doi : 10.1016/j.nima.2013.04.026.
- [31] T. Pöhlsen, Charge Losses in Silicon Sensors and Electric-Field Studies at the Si-SiO₂ Interface, Ph.D. thesis, University of Hamburg (2013).
URL <https://cds.cern.ch/record/1604839>
- [32] The Tracker Group of the CMS Collaboration, P-Type Silicon Strip Sensors for the new CMS Tracker at HL-LHC, JINST 12 (2017) P06018. doi : 10.1088/1748-0221/12/06/P06018.
- [33] The Tracker Group of the CMS Collaboration, Experimental study of different silicon sensor options for the upgrade of the CMS Outer Tracker, JINST 15 (2020) P04017. doi : 10.1088/1748-0221/15/04/P04017.
- [34] J.-O. Müller-Gosewisch, Investigation of Radiation Damage in Silicon Sensors for the Phase-2 Upgrade of the CMS Outer Tracker, Ph.D. thesis, KIT, Karlsruhe, ETP (2021).
URL <https://publish.etp.kit.edu/record/22097>